Soft Matter

Probing the swelling-dependent mechanical and transport properties of polyacrylamide hydrogels through AFM-based dynamic nanoindentation

Journal:	*Soft Matter*
Manuscript ID	SM-ART-11-2017-002351.R1
Article Type:	Paper
Date Submitted by the Author:	16-Feb-2018
Complete List of Authors:	Lai, Yang; University of Illinois at Urbana-Champaign, Department of Mechanical Science and Engineering Hu, Yuhang; University of Illinois at Urbana-Champaign, Department of Mechanical Science and Engineering

Soft Matter

PAPER

Probing the swelling-dependent mechanical and transport properties of polyacrylamide hydrogels through AFM-based dynamic nanoindentation

Received 00th January 20xx,
Accepted 00th January 20xx

DOI: 10.1039/x0xx00000x

www.rsc.org/

Yang Lai[a], Yuhang Hu[a]*

Hydrogels are composed of crosslinked polymer network and water. The constitutive behaviors of hydrogels have been modeled based on Flory-Huggins theory. Within the model, the thermodynamic and kinetic parameters are assumed to be constant values and typically characterized through swelling tests. Since most hydrogels can absorb a large amount of solvent from the dry state to swollen state, and the network size and solvent concentration of the hydrogels change significantly, the assumption of constant values of the thermodynamic and kinetic properties as the network swells is questionable. In this work, we experimentally show that even for the simple neutral polyacrylamide (PAAm) hydrogels, their mechanical responses cannot be fully described by the Flory-Huggins theory with constant thermodynamic parameters: N (number of chains per unit volume of dry polymers) and χ (polymer-solvent interaction parameter). For more complete and precise characterization of the hydrogels, we measure the evolving properties of the gels as the network swells. Here, we use dynamic indentation to measure the poroelastic properties (shear modulus G, Poisson's ratio v and diffusivity D) of the hydrogels under a wide range of swelling ratios. We also use linear perturbation to build the link between G v and N χ, and plot the thermodynamic parameters in the Flory-Huggins theory as functions of hydrogel swelling ratio. Consequently, the validity of the hydrogel models based on Flory-Huggins theory can be quantitatively examined.

Introduction

Gels are composed of crosslinked polymer networks and solvent molecules. If the solvent is water, the composite is called hydrogel. When a dry polymeric network is submerged in a solvent that has good chemical affinity with the polymers, the network tends to absorb the solvent to maximize the entropy, but meanwhile, the originally coiled polymer chains are straightened which also decrease the entropy of the composite. The competition of the two effects leads to an equilibrium state. From the dry to swollen states, gels can change volume dramatically. The solvent uptake is a two-way street: as the solvent diffuses into the network, the network deforms, leading to size and shape change, and meanwhile the deformation of the network also affects the rate and amount of solvent diffusing into or out of the network.

The flow-coupled deformation of hydrogels impart them with many unique applications in diverse engineering fields such as tissue scaffold[1], drug delivery[2], sensors and actuators[3–5], soft robotics[6,7], wearable electronics[8,9], microfluidics[10–12], packers in oil fields[13], and many others. The flow-coupled deformation of hydrogels is also intriguing to many mechanicians. Field theories of diffusion coupled deformation of hydrogels date back to Tanaka and his co-workers[14]. Lately, there have been several notable attempts to formulate a more physics based theory,[15–21] in which the nonequilibrium thermodynamics frame[22–25] has been formulated, leaving open the free-energy function and the kinetic laws, both of which are material specific. The thermodynamic part of the theory follows that of Flory and Rehner.[26–29] The crosslink density of the network is described by the parameter N (number of chains per unit volume of dry polymers), and the mixing behavior by the Flory-Huggins parameter χ (enthalpy of mixing). In the kinetic part, the flux was modeled as linearly proportional to the gradient of chemical potential with a constant diffusion coefficient D.[15–21,30] However, since most hydrogels can absorb large amount of solvent and the solvent concentration in the hydrogels changes dramatically as they evolve from dry to swollen states, the widely used assumption of constant N, χ and D is questionable. It is also believed to be one of the main reasons for that the models calibrated by one set of experiments often cannot predict the behaviors of the same hydrogel under different loading conditions.[16,18] Additionally, evidence has been seen in polymer solutions that both χ and D have strong dependence on solvent concentration due to a concentration dependence of chain mobility, solvent mobility and polymer-solvent interactions.[31–37] However, until now the parameters' dependence on solvent concentration (or equivalently the swelling ratio) of crosslinked hydrogels has rarely been studied.

[a] Department of Mechanical Science and Engineering, University of Illinois at Urbana-Champaign, Urbana, Illinois 61801, USA.

Alternatively, the Biot's poroelasticity (or biphasic model) has also been employed to describe the diffusion-coupled deformation of gels.[30,38–40] Different from Flory-Huggins theory, the materials' mechanical and transport behaviors in poroelasticity are characterized by the phenomenological parameters: shear modulus G, Poisson's ratio v, and diffusivity D. Based on this theory, in our previous work, we developed a dynamic indentation method that can characterize the poroelastic properties of the gels at particular swollen states. In this work, we will use Polyacrylamide (PAAm) hydrogel as a model material and use the dynamic indentation to characterize the poroelasticity (shear modulus G, Poisson's ratio v and diffusivity D) of the PAAm hydrogels at a wide range of swelling ratios. We will then link the mechanical part of the poroelastic properties (G, v) at each swelling ratio of the hydrogel to its thermodynamic properties in the Flory-Huggins theory: the effective crosslink density N, and polymer-solvent interaction parameter χ. Through this process, we can obtain the thermodynamic and kinetic parameters of the hydrogels as functions of the swelling ratio (or the solvent concentration) of the hydrogels. The validity of the Flory-Huggins theory with constant properties for the PAAm hydrogels is examined.

Experiment

To prepare the Polyacrylamide (PAAm) hydrogel samples, we first prepared the monomer solution by dissolving the Acrylamide in deionized water in 40% mass fraction, and the crosslinker solution by dissolving N,N'-Methylenebis(acrylamide) in deionized water in 2% mass fraction. The two solutions were mixed and further diluted by mixing with deionized water in the volume ratio of 3:3:14. We then added the initiator solution that was prepared by dissolving ammonium persulfate in deionized water in 10% mass fraction and the catalyst tetramethylethylenediamine into the mixture, in the volume fraction of 0.5% and 0.05% respectively. The mixture was then poured into a glass mold of 1 mm thick and was let set for 30 minutes. After the hydrogel was cured, the hydrogel samples were cut into small square pieces of 1×1cm^2 using a scalpel blade, and then fully immersed in deionized water for one day until it was fully saturated.

To prepare the PAAm hydrogels of different swelling ratios, we submerged the hydrogel samples prepared with the same composition as described above into the high molecular weight 1500 polyethylene glycol (PEG) solutions. Four concentrations of the PEG solutions were prepared with the mass fraction of 4.8%, 9.1%, 13.0%, and 16.7% respectively. Two groups of the PAAm hydrogel samples were submerged into each solution. One group was for swelling ratio measurement, and the other was for dynamic indentation measurement using Atomic Force Microscope (AFM). The volume of the PEG solution of each concentration was no less than 30 mL to ensure that the amount of water in the hydrogel samples had negligible effect on the concentration of the PEG solutions. The hydrogel samples were kept in the solutions for two days before testing to ensure that an equilibrium swelling state had been reached. The containers for the PEG solutions with PAAm samples were sealed before the experiments to avoid water evaporation.

Figure 1: Mechanical characterization of gels in different swelling ratios. (a) Indentation of gels using AFM. (b) The swelling ratio of the PAAm gel against the concentration of the external PEG solution.

In order to quantify the swelling ratio of the PAAm samples, the mass of each swollen PAAm sample and the mass of its dry polymer network were measured. First, the hydrogel samples were taken out of the PEG solution and weighed by a digital balance as the mass of the hydrogel. A tissue was gently applied on the gel surface to absorb the extra solution before weighing. The samples were then separately put into wells of a culture multiwall plate and lyophilized (FreeZone 6 Liter Benchtop Freeze Dry System) for two days. After lyophilization, the mass of each sample was measured by the digital balance again as the mass of the polymer network. The mass of the hydrogel at each swollen state is denoted as m_{hydrogel}, and its weight after dried is denoted as m_{polymer}. With the known polymer density ρ_{polymer}=1.443 g/cm^3,[41] and water density ρ_{water}=1.000 g/cm^3, the linear swelling ratio of the gel can be obtained as

$$\lambda = \left(1 + \left(\frac{m_{\text{hydrogel}}}{m_{\text{polymer}}} - 1\right) \cdot \frac{\rho_{\text{polymer}}}{\rho_{\text{water}}}\right)^{1/3} \quad (1)$$

Figure 1(b) plots the swelling ratio of the PAAm hydrogel λ as a function of the mass fraction of the external PEG solution. Its swelling ratio is around 2.8 in water and decreases as the mass fraction of PEG increases.

To characterize the linear mechanical and transport properties of the PAAm hydrogels at each swollen state, we

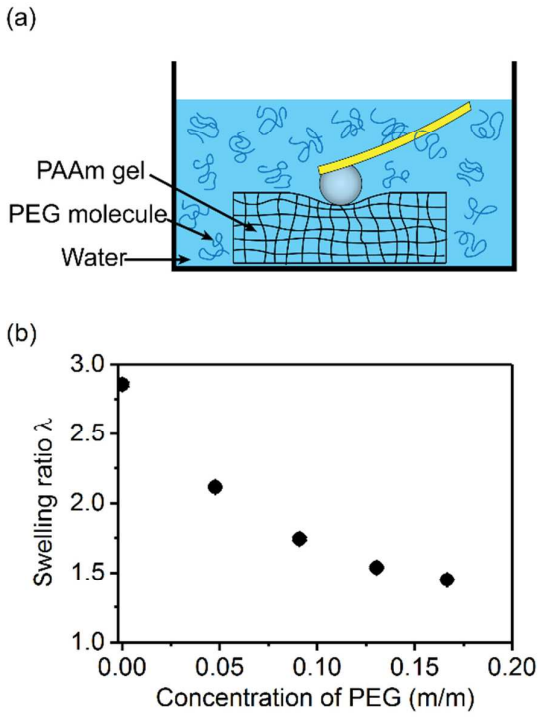

carried out dynamic oscillation indentation using AFM. As shown in Fig. 1(a), the dynamic indentation tests were conducted by Asylum Atomic Force Microscope. In the dynamic indentation measurement, the sample was submerged in solution throughout the test. A spherical indenter was pressed into the hydrogel to a depth h_0 (250 nm – 1 μm) and held for a period of time until the force on the indenter reached a constant value, $F(\infty)$. Then the indenter started an oscillation with a constant amplitude δh (20 nm) sweeping through a range of frequencies (0.2 – 40 Hz). The force response was recorded as a function of time $F(t)$. For oscillation, the time history of the applied indentation depth can be written as $h(t) = h_0 + \delta h \sin(\omega t)$, and the force response can be expressed as $F(t) = F(\infty) + F_a \sin(\omega t + \Delta)$, where F_a is the amplitude of the force response. The phase lag Δ between the force and displacement spectra indicates the energy dissipated in each cycle of loading and unloading. The following equation was used to calculate the phase lag degree from the raw data due to its simplicity in data processing[40].

$$\Delta = \arcsin\left(\frac{\oint F dh}{\pi F_a \delta h}\right). \qquad (2)$$

Details of the dynamic indentation tests using an atomic force microscope are as follows. The AFM tips used in the experiments are made of polystyrene sphere with diameter of 4.5 μm or 25 μm, and the cantilevers have spring constant ranging from 0.35 N/m to 1.00 N/m. The tips are purchased from Novascan. All the tests are carried out at least two days after the gels were immersed in PEG solutions. Before the AFM measurement, the PAAm sample is taken out of the PEG solution and glued to the petri dish. Enough amount of PEG solution is then added into the petri dish so that the sample is fully submerged in the PEG solution, and that the evaporated water from the solution is negligible during the test. Before indentation, the AFM tip is set to approach the sample surface at a speed of 2.5 μm/s. When a trigger value of 0.05 Volts is reached, the approaching is automatically switched to indenting with the speed of 50 μm/s until the initial indentation depth h_0 is reached, followed by the relaxation step and oscillation step. The applied displacement – time function is illustrated in Figure 2(a). It is carried out by the indentation mode of the Asylum AFM instrument. Both the indentation depth and the force on the indenter are recorded as functions of time for further analysis. The data acquisition rate is 2 kHz. The dynamic oscillation tests are carried out on several different spots on multiple hydrogel samples to ensure the statistical significance. On each sample, four different sizes of indentation are carried out, with the size of contact area spanning two orders of magnitudes. The results on phase lag as functions of actuation frequencies for the gel swollen in water and various PEG solutions are shown in Figures 2 and 3. Different from our previous work that the dynamic indentation is conducted under one frequency at a time and through different frequencies discretely, here to expedite the experiments, a sweeping frequency actuation is adopted: the frequency sweeps from 0.2 Hz to 40 Hz continuously while maintaining the same oscillation amplitude. On a piece of PAAm sample submerged in water, dynamic indentation measurement with constant frequency is also carried to check the validity of the sweeping frequency method. Figure 4 shows the results of the phase lag degree over oscillation cycles at

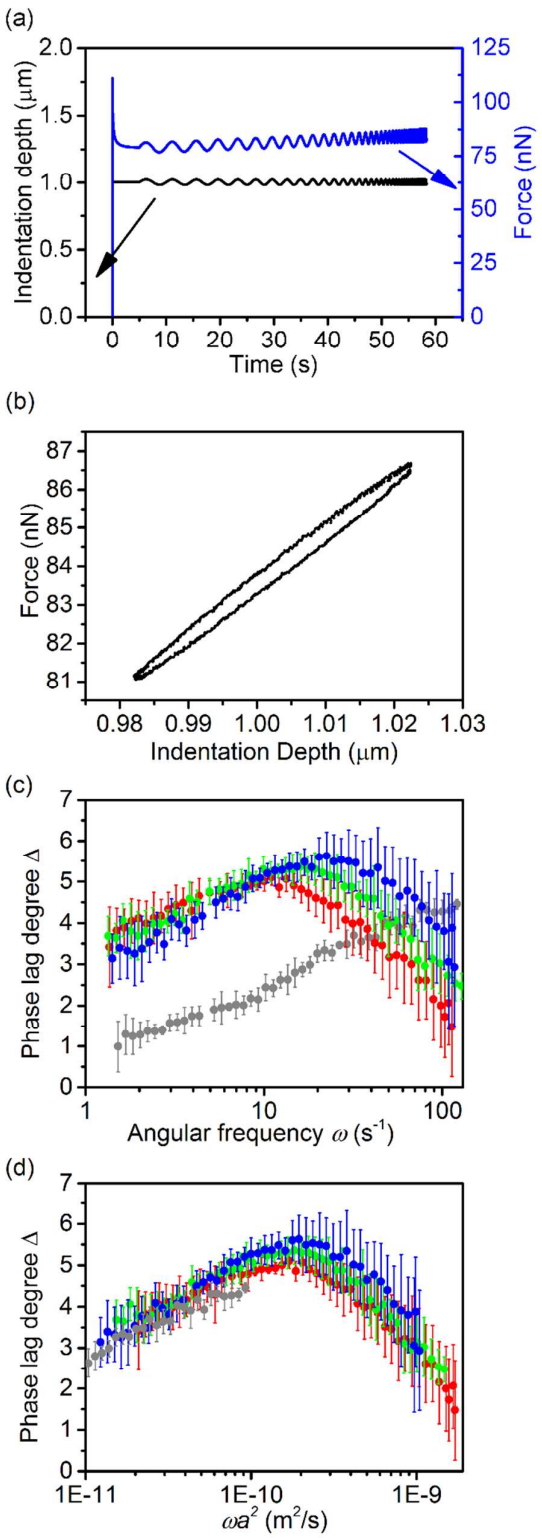

Figure 2: Dynamic indentation of PAAm gels swollen in pure water: (a) the displacement and force spectrums, (b) force response in one oscillation cycle at 1.22 Hz, (c) phase lag degree versus actuation angular frequency, (d) phase lag degree versus angular frequency times contact radius squared. The sphere radius and the indentation depth for each group of data are: red: R=12.5 μm, h_0=1.0 μm, green: R=12.5 μm, h_0=0.5 μm, blue: R=12.5 μm, h_0=0.25 μm, grey: R=2.25 μm, h_0=0.25 μm.

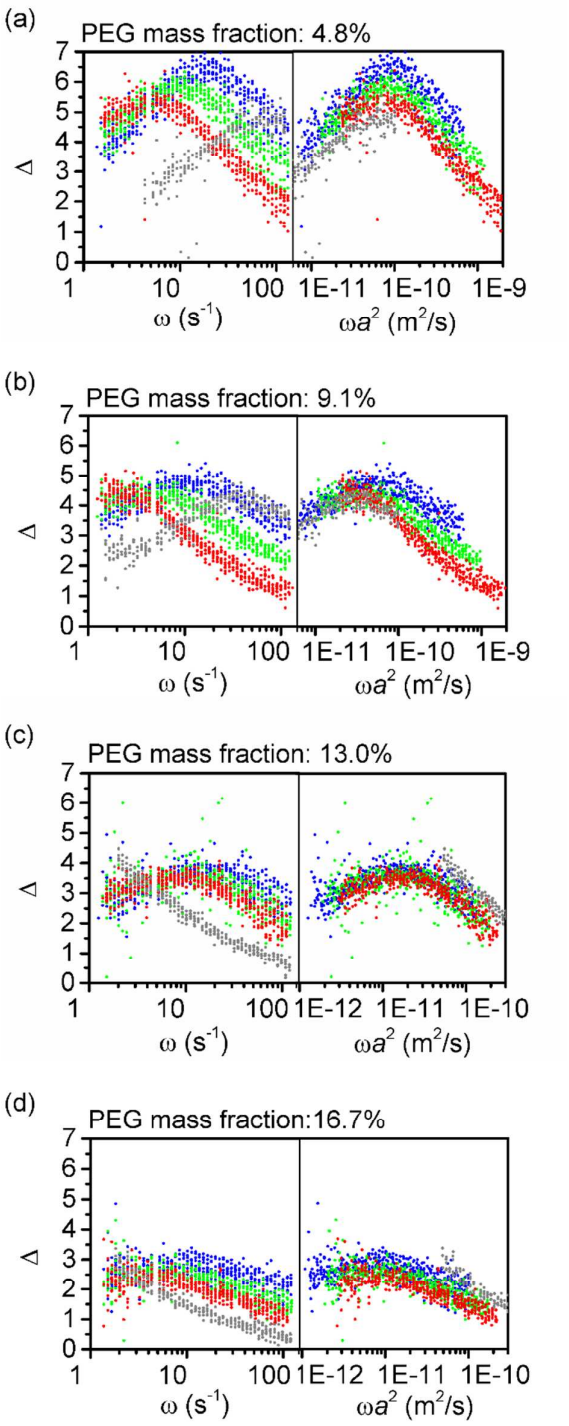

indentation depth of 500 nm for three fixed actuation frequencies, 0.6 Hz, 3.0 Hz and 32.0 Hz, representing low, medium and high frequencies in our testing range. The phase

Figure 3: Dynamic indentation of PAAm gels in PEG solutions of different concentrations. Sphere size and indentation depth for (a) and (b) are: Blue: R=12.5 μm, h_0=0.25 μm; Green: R=12.5 μm, h_0=0.5 μm; Red: R=12.5 μm, h_0=1.0 μm; Grey: R=2.25 μm, h_0=0.25 μm. Sphere size and indentation depth for (c) and (d) are: Blue: R=2.25 μm, h_0=0.25 μm; Green: R=2.25 μm, h_0=0.5 μm; Red: R=2.25 μm, h_0=0.75 μm; Grey: R=12.5 μm, h_0=2.0 μm.

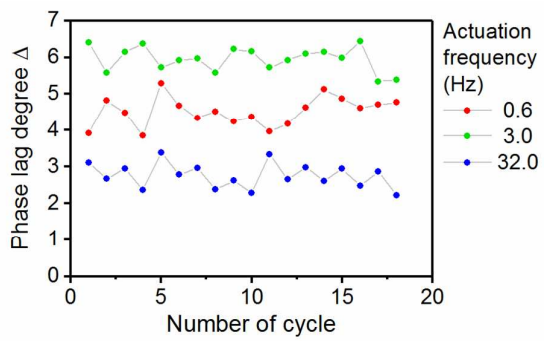

Figure 4: The phase lag degree measured in the dynamic indentation tests at three individual frequencies. The PAAm gel was swollen in water, and the indentation depth was around 500 nm.

lag degree for all three frequencies at the first cycle of oscillation is consistent with the values from subsequent cycles, and the phase lag values obtained from the constant frequency tests agree with those from the sweeping frequency tests at the equivalent frequencies.

To examine the possible adhesion between the tip and the PAAm hydrogel, we carry out an indenting-and-retracting test using the same tip. The test is conducted on a PAAm hydrogel in water. In the loading process, the indenting speed is set to be 50 nm/s, which is slow enough to ensure that the solvent in the hydrogel is equilibrated with the environment at all time. As is shown in Figure 5, the force-displacement curve obtained during the loading process fits very well with Hertzian model prediction, indicating very little to none adhesion. Following the loading, the tip is retracted at the same speed. The force-displacement curve obtained during the retraction process overlaps with the loading curve for the most part (Figure 5), except when the AFM probe is close to leave the hydrogel surface, and a nonzero pull-off force is observed. This observation of zero adhesion during approaching but nonzero pullout force during separation has also been observed before in the literature of nanoindentation of soft materials. [42,43] The reason is that for neutral hydrogels such as PAAm gels, the long range interaction between the polymer chains and the sphere that could contribute to the enlarged contact area is largely screened by water. Therefore, in experiment, we do not observe jump-to-contact during the approaching process. Only short range interaction is developed which only happens after the indenter is pressed into the sample. The short-range interaction does not induce the change of contact area but is responsible for the pull-out force after the indenter is retracted to leave the sample surface. In other words, the Hertzian contact model applies as long as the indenter does not retract. In the proposed dynamic oscillation, a deep indent (h=0.25, 0.5, 1, 2μm) is followed by a small amplitude oscillation (δh=20 nm), so the indenter is always in compression with the sample and the change of contact radius during oscillation is small enough to be neglected.[44] Consequently, since it is the information in the oscillation stage that we use to extract the poroelastic properties, the effect of adhesion between the spherical indenter and the hydrogel surface can be neglected. In fact, the possible short-

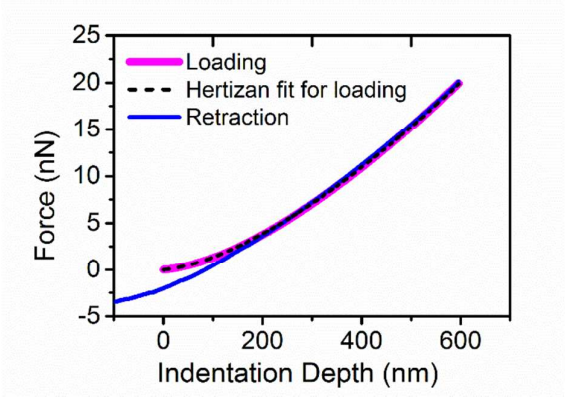

Figure 5: Loading and unloading curve from the AFM indentation test with speed of 50 nm/s. The Hertzian model fits well to the loading curve and most part of the unloading curve.

range adhesion between the very tip of the indenter and the sample may further stabilize the contact area to be a constant during oscillation. [45,46] This effect supports the treatment of constant contact radius in our method for extraction of poroelastic properties.

Discussions

The time dependent behavior of gels, in general, could be viscoelastic due to reconfiguration of polymer chains or poroelastic due to flow of solvent. An important character of poroelastic behavior from viscoelastic behavior is that the characteristic time scales of poroelastic behavior scales strongly with macroscopic length scale (for indentation problem, the length is the contact radius). As proposed in our previous work,[42] a simple method to differentiate the two time scales is through multi-depth indentation. If the phase lag spectrums obtained at different indentation depths collapse when the angular frequency ω is normalized as ωa^2, the energy dissipation of the gel is dominated by poroelasticity. Here a is the contact radius that equals $\sqrt{Rh_0}$ for spherical indenter with R being the radius of the sphere and h_0 the indentation depth, On the contrary, if the energy dissipation of the material is dominated by viscoelasticity, the curves from different depths of indentation will collapse in the $\Delta\sim\omega$ plot and separate in the $\Delta\sim\omega a^2$ plot.

Figure 2 shows one set of the measurement on the PAAm hydrogel swollen in pure water. The black and blue lines show the applied displacement and measured force spectrum respectively (Fig. 2a). Energy is dissipated through each cycle of loading and unloading (Fig. 2b), which can be used to calculate the phase lag value as in Eq. (2). The phase lag degree Δ is plotted as a function of angular frequency ω in Fig. 2(c). The red, green and blue lines are acquired from dynamic indentation using the sphere of radius 12.5 μm and indentation depth of 1, 0.5 and 0.25 μm, respectively. The curve shifts to the left as the indentation depth increases. When the angular frequency is normalized by the contact radius squared as ωa^2, the three groups of data overlap each other (Fig. 2d), which indicates that the time-dependent behavior of the swollen hydrogel is dominated by the flow of solvent.[44] These length scales are chosen because only in these length scales that we can capture the entire peak of the curve within the testing frequencies (0.1-100Hz) feasible for AFM. To convey the poroelasticity-dominant effect with more convincing evidence, we expand the probe length scale by using a sphere of 2.25 μm radius and depth of indentation of 0.25 μm. The curve is shown as the grey line in Fig. 2(c) and (d). Under this length scale, the peak of the curve falls out of the measurable frequency range of commercial AFM. Although the additional curve does not capture the complete up-and-down of the phase lag over measured frequencies, they show very obvious shift of characteristic time from the previous phase lag data (Fig. 2c). This length-dependent characteristic time is a signature of the poroelastic effect. It is further shown in Fig. 2(d) that when all the curves are plotted against the normalized actuation frequency, they collapse much better. If it is viscoelasticity-dominant effect, the curves should collapse in the phase-lag against frequency plot without normalization because viscoelastic time is independent of any macroscopic length. With the complete data sets across two orders of magnitudes in terms of contact area, it is convincing that the time-dependent response here is dominated by poroelastic effect.

Similar results are obtained for dynamic indentation of PAAm hydrogels in PEG solutions of 4.8%, 9.1%, 13% and 16.7% concentrations. Again, to capture the whole peak of phase lag, we first use sphere of 12.5 μm on the gels in 4.8% and 9.1% PEG solutions and sphere of 2.25 μm on the gel in 13% and 16.7% PEG solutions. Three depths of indentation are carried out for each case. The results are shown in Fig. 3 as the red, green and blue dots. Also in order to convey the poroelasticity-dominant effect with more convincing evidence, we expand the probe length scale for all the tests. Specifically, we add the data from 2.25 μm radius sphere on gel in the 4.8% and 9.1% PEG solutions and 12.5 μm radius sphere on the gel in 13% and 16.7% PEG solutions. The results are shown as the grey dots in Fig. 3. For all the experiments, the curves of the phase lag degree are separated when plotted as functions of actuation frequency, and they overlap each other when plotted as functions of normalized angular frequency.

At higher frequencies, there is slight deviation from a complete overlap of the phase lag curves when plotted against the normalized angular frequency. One possible reason is due to the hydrodynamic force on the AFM probe, the magnitude of which scales with the radius of the sphere and increases as the moving speed and the viscosity of the fluid.[47]. Another possible factor is the viscoelastic effect of the hydrogel, which is independent of any macroscopic length scale. Since the literature reported viscoelastic relaxation time of PAAm gel is around 0.01s[48], the viscoelastic effect may emerge at higher frequencies (>60 Hz). In spite of these factors, as our testing length scale changes an order of magnitude (4.5 μm to 25 μm sphere), the results from all the experiments in general collapse much better in the plot against normalized angular frequency comparing with the plot without normalization. Therefore, the conclusion can be drawn with confidence that

the measured time-dependent responses here are dominated by poroelastic effects.

Under small deformation, such as the shallow indentation in this work, the flow-coupled deformation of hydrogels can be modeled by linear poroelasticity, in which the constitutive relations of the material are described by shear modulus *G*, Poisson's ratio *v* and diffusivity *D*. The shear modulus indicates the hydrogel network's ability to resist to shear deformation. The Poisson's ratio indicates the ability of the network to retain solvent molecules after it reaches equilibrium under external mechanical and chemical loading. It is also referred as "drained Poisson's ratio" in geomechanics[49–51]. The diffusivity indicates the rate of solvent flow through the network.

In our previous work, unified solutions have been obtained that can be directly used to extract the linear poroelastic properties from the results of dynamic indentation measurements.[44] In the experiment, we obtain a spectrum of phase lag over a range of actuation frequency. If the energy dissipation captured by the indentation measurement is due to poroelastic effect, the magnitude of phase lag indicates the magnitude of the energy dissipated as the solvent molecules flows in and out of the polymer network. Therefore, the peak value of the phase lag Δ_c captured in experiment can be used to extract the Poisson's ratio of the material. Corresponding to the peak phase lag, the critical angular frequency ω_c is related to a characteristic time scale of the material. For poroelastic material, the characteristic time is related to how fast the solvent molecules transport through the network. Therefore, the value of the critical angular frequency can be used to extract the diffusivity value of the material. Here we list the steps summarized in our previous work to calculate the linear poroelastic properties of the hydrogels.

The Poisson's ratio *v* can be calculated from the value of the critical phase lag value Δ_c using the following equation:

$$\nu = g_1(\Delta_c) = 0.5 - 0.027\Delta_c - 0.00136\Delta_c^2 . \qquad (3)$$

Comparing the experimentally measured critical angular frequency ω_c corresponding to the peak of the phase lag with the theoretical value of the normalized critical angular frequency Ω_c that can be obtained from the master equation

$$\Omega_c = g_2(\nu) = 1.975 + 0.872\nu + 1.605\nu^2 , \qquad (4)$$

we can obtain the diffusivity of the material as

$$D = \frac{a^2\omega_c}{\Omega_c} . \qquad (5)$$

Finally, the shear modulus is obtained from the relaxed force, $F(\infty)$ which is measured after a period of initial indent and before the oscillation is applied. Here Hertzian's solution can be used considering the material behaves as a compressible material in the equilibrium state:

$$G_s = \frac{3(1-\nu)F(\infty)}{8h_0 a} . \qquad (6)$$

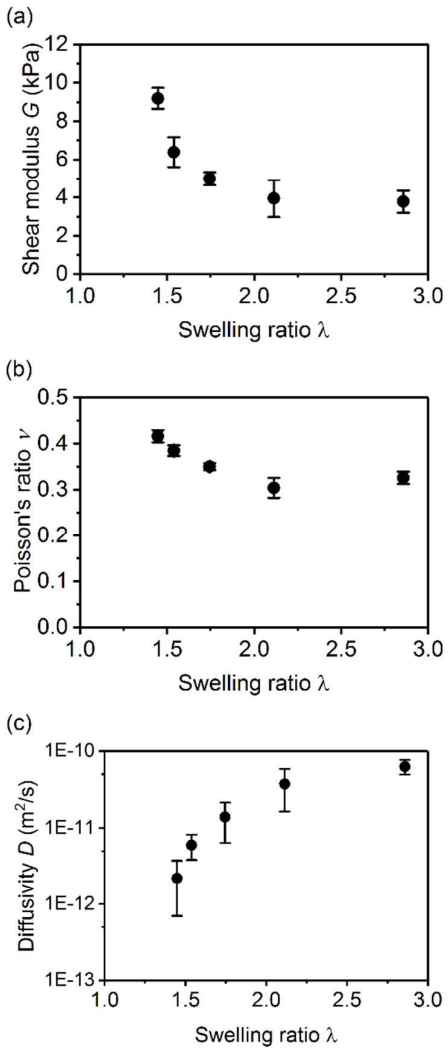

Figure 6: Linear poroelastic properties of the PAAm gels: (a) shear modulus, (b) Poisson's ratio and (c) diffusivity against swelling ratios.

Figure 6 shows the result of the shear modulus *G*, Poisson's ratio *v* and diffusivity *D* as functions of swelling ratio *λ*, with the error bars being the standard deviation from nine tests. The shear modulus decreases as the swelling ratio increases, because the network density is lower and its ability to resist deformation is lower. The Poisson's ratio decreases as the swelling ratio increases. When the solvent content is high in the gel, more solvent can flow into or out of the gel to cause the volume change, and vice versa. The result also shows that the diffusivity of the gel increases two orders of magnitude from the scale of 10^{-12} m^2/s to 10^{-10} m^2/s as its swelling ratio only changes two times from 1.4 to 2.8.

The nonlinear model that is supposed to describe the behaviors of gels all the way from dry to swollen states has been derived based on the Flory-Huggins theory,[26,27,29,52,53] according to which the free energy of a gel is a summation of the stretching energy and mixing energy,

$$W=\frac{1}{2}Nk_BT\left\{\mathrm{Tr}(\mathbf{F}^{\mathrm{T}}\mathbf{F})-3-\ln\left[\det(\mathbf{F})\right]\right\} -\frac{k_BT}{\Omega}\left(\Omega C\ln\left(1+\frac{1}{\Omega C}\right)+\frac{\chi}{1+\Omega C}\right) \quad (7)$$

where $\boldsymbol{F}_{iK}=\partial x_i/\partial X_K$ is the deformation gradient with $\boldsymbol{X}$ being the reference coordinates and $\boldsymbol{x}(\boldsymbol{X},t)$ the current coordinates, N the number of polymer chains per unit volume of the dry polymer, k_B the Boltzmann constant, T the temperature, Ω the volume of a solvent molecule, C the number of solvent molecules per unit volume of the dry polymer, and χ the Flory-Huggins interaction parameter. Assuming the individual polymer chains and solvent molecules are incompressible, we have $1+\Omega C=\det(\boldsymbol{F})$. [13,18,39] Here the stretching energy follows the incompressible Neo-Hookean model, in which the deformation of each polymer chain follows Gaussian statistics and the total free energy is the summation of the stretching energy of all the polymer chains. The mixing energy was derived by Flory and Huggins based on the similar statistics for binary solutions.[27]

It has to be mentioned that gels can absorb large amount of solvent and have huge volume change. The model in equation (7) has been used to describe the large deformation of gels evolving from the dry to swollen states. However, indentation is induced at a particular swollen state of the gel. The deformation induced by indentation is small. Therefore, the deformation of the gel under indentation at a particular swollen state can be modeled by linear poroelasticity. It has to be pointed out that, the linear poroelasticity only works for the gel's behavior in the vicinity of this particular swollen state, but would not work for the whole large volume change of the gel. The poroelastic properties measured at these particular swollen states of gels can be viewed as the incremental properties of the gels at each swollen state. The overall goal of this study is to obtain the mechanical and transport properties of a model hydrogel under different swelling ratios, and to examine the applicability of the large deformation model based on the Flory-Huggins theory for the whole range of deformations of gels from the dry state all the way to the swollen state.

To link the measured linear poroelastic properties of the gels to their thermodynamic properties in the nonlinear model, we linearize the nonlinear theory around a particular swollen state of the gel $\lambda=\sqrt[3]{1+C\Omega}$, and compare it with linear poroelasticity, the free energy of which is expressed as

$$w=G\left[\varepsilon_{ij}\varepsilon_{ij}+\frac{\nu}{1-2\nu}(\varepsilon_{kk})^2\right] \quad (8)$$

As a result, we obtain the following relations to link the shear modulus and Poisson's ratio to the thermodynamic parameters N and χ for this particular swelling ratio, λ as:

$$\frac{Nk_BT}{2}\left(\frac{1}{\lambda}+\frac{1}{\lambda^3}\right)+\frac{k_BT}{2\Omega}\left[\ln\left(\frac{\lambda^3}{\lambda^3-1}\right)-\frac{1}{\lambda^3}-\frac{\chi}{\lambda^6}\right]=G, \quad (9)$$

$$\frac{\lambda^6-\chi\left(\lambda^3-1\right)-\lambda^6\left(\lambda^3-1\right)\ln\left(\frac{\lambda^3}{\lambda^3-1}\right)}{\left(\lambda^3-1\right)\left[-\chi-\lambda^3+N\Omega\lambda^3\left(\lambda^2+1\right)+\lambda^6\ln\left(\frac{\lambda^3}{\lambda^3-1}\right)\right]}=\frac{\nu}{1-2\nu} \quad (10)$$

An interesting observation from Eq. (9) is that the shear modulus of the hydrogel at a particular swelling ratio is not only related to the stretching state of the polymer network (the first term in equation (9) with N), but also the mixing between the polymer network and the solvent (the second term in equation (9) with χ). This dual contribution from both stretching and mixing to the gels' resistance to deformation may lead to an unexpected trend of shear modulus of the gel as it swells or shrinks. As shown in Fig. 6a, the measured shear modulus of the gel decreases from 9.2 kPa to 3.9 kPa as the gel swells from 1.4 to 2.1 in linear swelling ratio, but does not decrease further as the gel swells further from 2.1 to 2.8. From the swelling ratio of 2.1 to 2.8, the contribution of the polymer chains to the gel's resistance to deformation decreases while the contribution of the mixing term increases. Consequently, the hydrogels with significantly different swelling ratios have similar shear modulus.

Substituting the measured $G(\lambda)$ and $\nu(\lambda)$ of the PAAm hydrogel into Eqs. (9) and (10), we can calculate $N(\lambda)$ and $\chi(\lambda)$ of the same gel. As shown in Fig. 7(a), N keeps increasing as the swelling ratio decreases, which indicates that additional crosslinking mechanism such as the entanglement of the polymers may also contribute to the effective crosslink of the hydrogel at lower swelling ratios. As shown in Fig. 7(b), χ is close to 0.5 at high swelling ratio, and increases as swelling ratio decreases. This result suggests that the Flory-Huggins interaction parameter χ strongly depends on the polymer concentration,[35,37] which is a known phenomenon for polymer solutions, but is the first time that is captured and quantified for the crosslinked PAAm hydrogels. The result suggests that it is not just the free energy function being less than perfectly accurate or the systematic error from experiment. If we assume the free energy function form is correct, then the modification for N value has to change three orders of magnitude (1e24-1e27) and the modification of χ is from 0.9 to 0.4 which is also big.

The possible mechanisms that are commonly considered for modifying the Flory-Huggins theory include the large stretching induced stiffening of the polymer chains[54–56] and the possible interactions between the polymer chains, such as entanglements[57,58]. When the polymer chains inside the network are significantly stretched, the Gaussian statistics model is no longer sufficient to describe the chain's behavior. Previous studies have implemented this effect in the chain model, such as the Arruda-Boyce model based on the Langevin statistics.[55] The stretching limit beyond which the Gaussian statistics model fails increases with the number of monomers between two crosslinkers[27,55]. The exact value of the stretching limit for PAAm hydrogels with similar monomer and crosslinker concentration has been studied in our previous work[59,60], which is above 3 and is higher than the maximum swelling ratio (i.e. 2.8) in this work. Only when the PAAm network is modified to become polyelectrolyte, the stretching induced stiffening of the chain needs to be considered. Therefore,

the stiffening effect can be neglected in the experiments of this work. On the other hand, as the swelling ratio of the gel decreases, the possibility for the polymer chains to interact with each other increases. As shown in Fig. 7a, the value of *N* increases dramatically as swelling ratio of the gel decreases, indicating the entanglement between chains may be formed.

The diffusivity of the solvent transporting through the network indicates a characteristic length of the polymeric network – the effective pore size. Considering the polymeric network as a porous media, its flow kinetics can be modeled by Darcy's law[49] and the diffusivity of the solvent can be related to the permeability *k* of the porous skeleton as

$$k = \frac{(1-2\nu)}{2(1-\nu)}\frac{D\eta}{G}, \qquad (11)$$

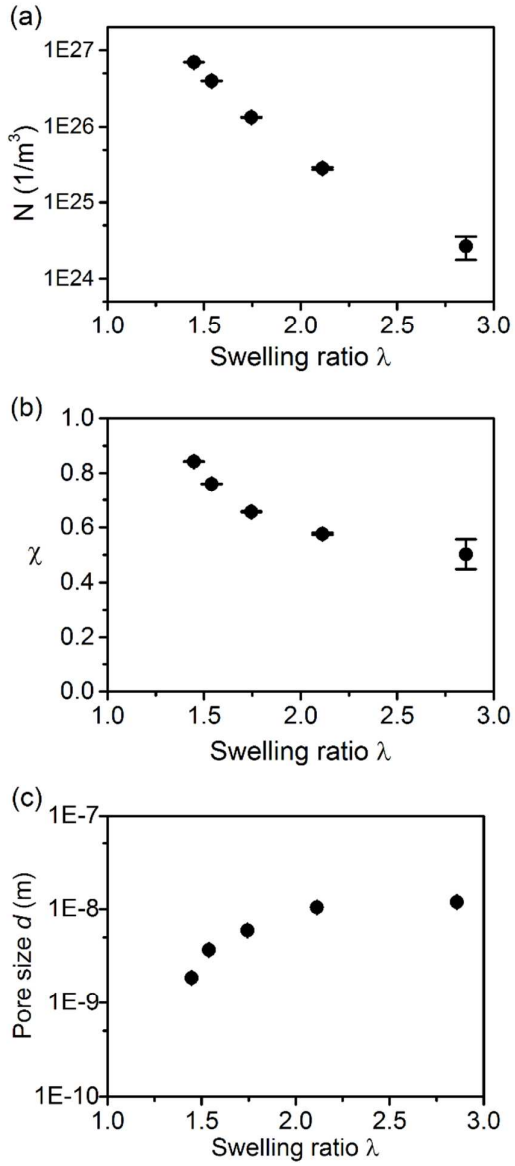

Figure 7: Thermodynamic properties of the PAAm gels: (a) the parameter N, (b) the Flory-Huggins interaction parameter χ, and (c) the effective pore size for solvent transport d, against swelling ratios.

where η is the viscosity of the solvent. The permeability parameter has a unit of length squared. To link it to the pore size, we need a micro-structural model. Adopting the simplest one that assumes the liquid transport pathways are in the form of a series of parallel cylindrical tubes,[61] the diameter of the cylindrical tubes can be expressed as

$$d^2 = \frac{32k\tau^2}{\varphi} \qquad (12)$$

where φ is the porosity (i.e. the ratio between the pore volume to the overall volume), and τ the tortuosity. We assume the tortuosity depends on the porosity φ as $\tau = \varphi^{-\beta}$, where β is a parameter related to the pore geometry[62–64]. For the fully swollen gel, more than 95% content is water, so the tortuosity value is close to 1. When the network is dry with the porosity of 7.86%, the tortuosity is taken to be round 15 as for dry polymeric networks.[65] Substituting these data gives $\beta = 1.068$.

The magnitude of the effective pore size is plotted in Fig. 7(c), the pore size of the hydrogel fully swollen in water is on the order of 10 nm, and the value decreases in small swelling ratio regions. In general, the result shows a nonlinear change in the pore size with respect to swelling ratio. This result provides quantitative data for further studies of the molecular mechanisms of gel kinetics.

Conclusion

In this study, we choose PAAm hydrogel as a model material and experimentally measured its property dependence on the swelling ratio (or equivalently the solvent concentration). The results indicate that the deformation mechanism of gels goes beyond the original Flory-Huggins theory, even for the simple neutral PAAm hydrogel. This work is expected to inspire more study of the deformation mechanism of hydrogels in the future.

Acknowledgements

This work was supported by the National Science Foundation under Grant No. 1554326. The oscillation indentation tests were carried out in the Frederick Seitz Materials Research Laboratory Central Research Facilities, University of Illinois.

Notes and references

1 J. L. Drury and D. J. Mooney, *Biomaterials*, 2003, **24**, 4337–4351.
2 B. B. V Slaughter, S. S. Khurshid, O. Z. Fisher, A. Khademhosseini and N. A. Peppas, *Adv. Mater.*, 2009, **21**, 3307–3329.
3 D. Buenger, F. Topuz and J. Groll, *Prog. Polym. Sci.*, 2012,

37, 1678–1719.
4 A. Richter, G. Paschew, S. Klatt, J. Lienig, K.-F. Arndt and H.-J. P. Adler, *Sensors*, 2008, **8**, 561–581.
5 G. Gerlach, M. Guenther, J. Sorber, G. Suchaneck, K. F. Arndt and A. Richter, *Sensors Actuators B Chem.*, 2005, **111–112**, 555–561.
6 P. Calvert, *Adv. Mater.*, 2009, **21**, 743–756.
7 D. Morales, E. Palleau, M. D. Dickey and O. D. Velev, *Soft Matter*, 2014, **10**, 1337–1348.
8 Z. Chen, J. W. F. To, C. Wang, Z. Lu, N. Liu, A. Chortos, L. Pan, F. Wei, Y. Cui and Z. Bao, *Adv. Energy Mater.*, 2014, **4**, 1–10.
9 S. Lin, H. Yuk, T. Zhang, G. A. Parada, H. Koo, C. Yu and X. Zhao, *Adv. Mater.*, 2016, **28**, 4497–4505.
10 D. J. Beebe, J. S. Moore, J. M. Bauer, Q. Yu, R. H. Liu, C. Devadoss and B. Jo, *Nature*, 2000, **404**, 588–590.
11 L. Dong, A. K. Agarwal, D. J. Beebe and H. Jiang, *Nature*, 2006, **442**, 551–554.
12 M. P. Cuchiara, A. C. B. Allen, T. M. Chen, J. S. Miller and J. L. West, *Biomaterials*, 2010, **31**, 5491–5497.
13 S. Cai, Y. Lou, P. Ganguly, A. Robisson and Z. Suo, *J. Appl. Phys.*, 2010, **107**, 1–7.
14 T. Tanaka and D. J. Fillmore, *J.Chem. Phys.*, 1979, **70**, 1214–1218.
15 C. J. Durning and K. N. Morman, *J. Chem. Phys.*, 1993, **98**, 4275–4293.
16 M. Doi, *J. Phys. Soc. Japan*, 2009, **78**, 1–19.
17 H. Ji, H. Mourad, E. Fried and J. Dolbow, *Int. J. Solids Struct.*, 2006, **43**, 1878–1907.
18 W. Hong, X. Zhao, J. Zhou and Z. Suo, *J. Mech. Phys. Solids*, 2008, **56**, 1779–1793.
19 F. P. Duda, A. C. Souza and E. Fried, *J. Mech. Phys. Solids*, 2010, **58**, 515–529.
20 S. A. Chester and L. Anand, *J. Mech. Phys. Solids*, 2011, **59**, 1978–2006.
21 N. Bouklas and R. Huang, *Soft Matter*, 2012, **8**, 8194–8203.
22 J. W. Gibbs, *The Scientific Papers of J. Willard Gibbs*, 1878.
23 M. A. Biot, *Int. J. Solids Struct.*, 1977, **13**, 579–597.
24 I. Prigogine, *Introduction to Thermodynamics of Irreversible Processes, third ed*, Wiley, New York, 1967.
25 B. D. Coleman and W. Noll, *Arch. Ration. Mech. Anal.*, 1963, **13**, 167–178.
26 P. J. Flory, *J. Chem. Phys.*, 1942, **10**, 51–61.
27 P. J. Flory, *Principles of polymer chemistry*, Cornell University Press, 1953.
28 P. J. Flory and J. Rehner, *J. Chem. Phys.*, 1943, **11**, 521–526.
29 M. L. Huggins, *J. Chem. Phys.*, 1941, **9**, 440.
30 G. W. Scherer, *J. Am. Ceram. Soc.*, 2000, **83**, 2231–2239.
31 D. W. van Krevelen, *Properties of polymers*, Amsterdam: Elsevier, 1990.
32 E. H. I. J. Brandrup, *Polymer handbook (3rd ed.)*, Wiley, New York, 1989.
33 A. F. M. Barton, *CRC-handbook of polymer–liquid interaction parameters and solubility parameters*, CRC press, Boca Raton, 1990.
34 J. E. Mark, *Physical properties of polymers handbook*, American Institute of Physics, Woodbury, 1996.
35 R. A. Orwoll, *Rubber Chem. Technol.*, 1977, **50**, 451–479.
36 N. A. Peppas and E. W. Merrill, *J. Polym. Sci. Polym. Chem. Ed.*, 1976, **14**, 459–464.
37 A. G. Mikos and N. A. Peppas, *Biomaterials*, 1988, **9**, 419–423.
38 Y. Hu and Z. Suo, *Acta Mech. Solida Sin.*, 2012, **25**, 441–458.
39 S. Cai, Y. Hu, X. Zhao and Z. Suo, *J. Appl. Phys.*, 2010, **108**, 1–8.
40 W.-C. Lin, K. R. Shull, C.-Y. Hui and Y.-Y. Lin, *J. Chem. Phys.*, 2007, **127**, 94906.
41 S. Cai and Z. Suo, *EPL*, 2012, **97**, 8121–8128.
42 P. C. Nalam, N. N. Gosvami, M. A. Caporizzo, R. J. Composto and R. W. Carpick, *Soft Matter*, 2015, **11**, 8165–8178.
43 Y. M. Efremov, D. V. Bagrov, M. P. Kirpichnikov and K. V. Shaitan, *Colloids Surfaces B Biointerfaces*, 2015, **134**, 131–139.
44 Y. Lai and Y. Hu, *Soft Matter*, 2017, **13**, 852–861.
45 K. R. Shull, *Contact mechanics and the adhesion of soft solids*, 2002, vol. 36.
46 K. J. Wahl, S. A. S. Asif, J. A. Greenwood and K. L. Johnson, *J. Colloid Interface Sci.*, 2006, **296**, 178–188.
47 J. Alcaraz, L. Buscemi, M. Puig-De-Morales, J. Colchero, A. Baro and D. Navajas, *Langmuir*, 2002, **18**, 716–721.
48 N. Weiss and A. Silberberg, *Br. Polym. J.*, 1977, **9**, 144–150.
49 M. A. Biot, *J. Appl. Phys.*, 1941, **12**, 155–164.
50 K. von. Terzaghi, *Sitzungsberichte der Akad. der Wissenschaften Wien, Math. Klasse, Abteilung IIa*, 1923, **132**, 125–138.
51 J. R. Rice and M. P. Cleary, *Rev. Geophys. Sp. Phys.*, 1976, **14**, 227–241.
52 Y. Hu, X. Chen, G. M. Whitesides, J. J. Vlassak and Z. Suo, *J. Mater. Res.*, 2011, **26**, 785–795.
53 P. J. Flory, *Trans. FARADAY Soc.*, 1960, **57**, 829–838.
54 A. N. Gent, *RUBBER Chem. Technol.*, 1996, **69**, 59–61.
55 E. M. Arruda and M. C. Boyce, *J. Mech. Phys. Solids*, 1993, **41**, 389–412.
56 M. C. Boyce and E. M. Arruda, *Rubber Chem. Technol.*, 2000, **73**, 504–523.
57 L. R. G. Treloar, *The physics of rubber elasticity*, Oxford University Press, USA, 1975.
58 M. Doi and S. F. Edwards, *Claredon, Oxford.*, 1986, **6**.
59 J. Li, Y. Hu, J. J. Vlassak and Z. Suo, *Soft Matter*, 2012, **8**, 8121–8128.
60 J. Li, Z. Suo and J. J. Vlassak, *Soft Matter*, 2014, **10**, 2582.
61 X. Hou, Y. Hu, A. Grinthal, M. Khan and J. Aizenberg, *Nature*, 2015, **519**, 70–73.
62 G. E. Archie, *Trans. AIME*, 1942, **146**, 54–62.
63 L. Pisani, *Transp. Porous Media*, 2011, **88**, 193–203.
64 B. Ghanbarian, A. G. Hunt, R. P. Ewing and M. Sahimi, *Soil Sci. Soc. Am. J.*, 2013, **77**, 1461–1477.
65 K. Kulasinski and R. A. Guyer, *J. Phys. Chem. C*, 2016, **120**, 28144–28151.

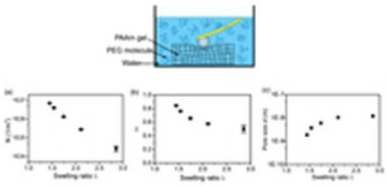

16x8mm (300 x 300 DPI)